Step Towards Energy-Water Smart Microgrids; Buildings Thermal Energy and Water Demand Management Embedded in Economic Dispatch

Faegheh Moazeni, Javad Khazaei, *Senior Member, IEEE*, and Arash Asrari, *Senior Member, IEEE*

***Abstract*—Energy, building, and water networks are three interlinked critical infrastructures that need to be operated cooperatively to maximize the smart grid's economic benefits. In this paper, a mixed-integer linear programming (MILP) formulation is proposed to approach the economic dispatch (ED) problem for smart grids embedded with interdependent water and energy networks. Energy management of various building applications is considered by intelligently controlling the indoor temperature during occupied and unoccupied hours. To optimize the demand of water distribution system, pump's nonlinear scheduling and hydraulic factors and daily water usage of buildings are added to the proposed model. Piecewise linear approximation of univariate and bivariate nonlinear functions is used to convert the nonlinear problem to an MILP formulation. Several case studies were conducted to examine the impact of indoor temperature settings of the buildings, speed of pumps, battery efficiency, and end of day (EoD) battery and tank constraints on economic dispatch of the microgrid system.**

***Index Terms*—Economic Dispatch, Mixed Integer Linear Programming (MILP), Piecewise Linearization, Thermal Equilibrium, Water Demand Management.**

NOMENCLATURE

P_{grid}	Output grid power.
$f(P_G), P_G$	cost and power of conventional DGs.
C_{up}, C_{dn}	Startup and shutdown costs.
C_C, C_P	Cost functions of chillers and pumps.
S_{up}, S_{dn}	Startup and shutdown status of DGs.
$f_{pv}, f_{wind}, f_{batt}$	Cost functions of PV plant, wind farm, and battery energy storage units.
P_{PV}, P_{wind}, P_{batt}	Output power of PV plant, wind farm, and battery energy storage units.
P_{chil}, P_{pump}	Power of chillers and pumps.
U_{DG}	Status of DG unit
R_{up}^{max}, R_{down}^{max}	Maximum ramp up and down limits.
K_{wind}, K_{PV}, K_{batt}	Cost coefficient of the wind, solar, and battery units, respectively.
E_{batt}	Energy level of the battery storage.
Q_{wall},Q_{win}	Heat gains of walls and windows.
Q_{chil}	Cooling power of chillers.
U_{wall}, U_{win}	Heat transfer coefficient of the walls and windows.
A_{wall}, A_{win}	Area of the walls and windows.
T_{in}, T_{out}	Indoor and outdoor temperatures.
$Q_{m,n}$	Flow rate between nodes m and n.
S	Status of the pump.
Δh	Head gain of the pump.
Q_R	Flow rate from the reservoir.
Q_T	Volume of water in the tank.
Q_D	Water demand.
H_m, H_n	Pressure head at nodes m and n.
$\mathcal{P}$	Linearized function of pump's power.
$\mathcal{H}$	Linearized function of pump's gain.
r	Variable speed of the pump.

Manuscript received April 10, 2020; revised September 15, 2020 and January 23, 2021; accepted March 15, 2021. Date of publication March 22, 2021; date of current version August 23, 2021. Paper no. TSG-00533-2020. *(Corresponding author: Javad Khazaei.)*

Faegheh Moazeni is with the Civil and Environmental Engineering Department, Penn State Harrisburg, Middletown, PA 17057 USA (e-mail: fxm53@psu.edu).

Javad Khazaei is with the Electrical Engineering Department, Penn State Harrisburg, Middletown, PA 17057 USA, and also with the Architectural Engineering Department, Penn State University, State College, PA 16801 USA (e-mail: jxk792@psu.edu).

Arash Asrari is with the School of Electrical, Computer, and Biomedical Engineering, Southern Illinois University, Carbondale, IL 62901 USA (e-mail: arash.asrari@siu.edu).

Color versions of one or more figures in this article are available at https://doi.org/10.1109/TSG.2021.3068053.

Digital Object Identifier 10.1109/TSG.2021.3068053

I. INTRODUCTION

ENERGY and water systems are intertwined; 15% of global water is consumed for cooling purposes in thermal power plants and water distribution and treatment centers consume 8% of global energy [1]. Therefore, due to the scarcity of water and pollution issues resulted by thermal power plants, the performance of interlinked energy-water networks must be optimized in a cooperative manner. Several research works focused on minimizing the water demand and energy consumption of integrated energy-water systems [2]–[7]. These studies, however, did not focus on the fact that future energy generation will significantly depend on renewable energy sources and storage units and merely rely on conventional fossil-fuel-based generation. In addition, these studies did not incorporate the building sector in the formulation nor optimized the water consumption. To account for future energy supplies and distribute energy in smart water-energy system, the concept of water-energy microgrid has recently been introduced [8]. Several studies focused on the application of microgrids for water-energy systems to address the future needs of interlinked energy-water systems [9]–[14]. For example, an approach was proposed in [9] to promote remote

communities in Alaska to use microgrids and increase the resiliency of integrated food-energy-water systems. A stochastic energy management program was supplemented to the distribution system operator (DSO) in [10] to maximize the reliability of water-energy systems by restoring disconnected loads during emergency. This work, however, mainly focused on the energy supply and did not consider the details of water distribution system or building sector. Control of a hybrid microgrid composed of a diesel generator and a wind turbine for a water treatment facility was studied in [11]. The proposed method provided an energy-demand balance during wind speed changes or load change events. This work, however, did not consider dynamics of the load nor water distribution system. Potential of seawater desalination using energy surpluses of microgrids with renewable energy sources and thermosolar absorption cooling system for an isolated community in Mexico was demonstrated in [12]. Similar to other works, the study did not consider water distribution systems nor thermal management of buildings. In the authors' recent research, a mixed integer nonlinear programming (MINLP) formulation was proposed to optimize the water consumption in an energy-water microgrid with renewable energy sources and storage devices [13]. However, it did not focus on thermal management of the buildings.

Contributions: Existing studies have made reasonable contributions towards the economic dispatch of combined water-energy microgrids, there are still a few unanswered questions and gaps that require more research. While the theories and fundamentals applied in power system, hydraulic design (e.g., mass and energy continuity theorem), and transfer phenomenon (heat transfer equations) are well-studied, these theorems have been independently implemented for individual systems, while the interlinks and interdependence between these systems and their impacts on the overall performance of the integrated system have not been considered before. For example, the relationship between heating/cooling demands of the buildings, customer's temperature comfort range and impact of outdoor temperature on demand response has not been considered in integrated water-energy networks yet. Moreover, the nonlinear nature of pumps in water distribution system does not guarantee a global optimum in resource allocation problem. In addition, operating conditions of pumps in water distribution systems significantly affect the daily electricity cost and have to be added to the formulation. In this research, it is shown how optimization of every component belonging to a subsystem can have a large impact on the overall cost, power consumption, and resource allocation of the entire system. The main contributions of this research are listed in the following:

- A day-ahead economic dispatch model of an energy-water microgrid supplying electrical load of various building types and water distribution system is formulated.
- Thermal equilibrium of buildings is added to the formulation to optimize the operation of cooling devices in the microgrid considering customer's comfort range and outdoor temperature and solar radiation forecast.
- The energy consumption of water distribution system is minimized by formulating the conservation of mass and Bernoulli's energy equations.
- The nonlinearities of the thermal equilibrium in building sector, conservation of mass and energy theorem in water distribution networks, and cost functions of conventional generation plants are linearized using piecewise linear approximation method.
- The effect of indoor temperature settings, pump's speed, battery efficiency, and end-of-day (EoD) battery/tank levels on economic operation of energy-water microgrid is studied in various scenarios.

The problem formulation is included in Section II and energy management of generation units is included in Section III. Section IV elaborates the buildings' thermal management, and water distribution management is included in Section V. Case studies are included in Section VI and Section VII concludes the paper.

II. Problem Formulation

The system under investigation, as shown in Fig. 1, is a microgrid with energy resources including three distributed generation (DG) units, an aggregated battery energy storage system (BESS), an aggregated photovoltaic (PV) plant, and an aggregated wind farm. Both grid-connected and islanded modes of operation are considered to enable buying/selling electricity from/to the grid. Loads include three types of buildings including a residential house, an office, and an apartment complex. The water distribution system is a seven-node system with one reservoir, one tank, and one pump to support the water demand of the system. The economic dispatch problem is formulated as a mixed integer linear programming (MILP) formulation. The microgrid energy management system in Fig. 1 receives measurements from the energy sources and loads and runs the proposed economic dispatch formulation to minimize the overall cost of the system considering resource allocation in microgrid, control of chillers in the buildings, and control of pumps in water distribution network.

1) Objective Function: The objective is to minimize the operation cost of an energy-water system by reducing the power consumption of the pumps in the water distribution network and electric chillers in the energy-water system.

$$\min \sum_{t\in T}\Bigg\{\left(\frac{C^t_{buy}+C^t_{sell}}{2}P^t_{grid}+\frac{C^t_{buy}-C^t_{sell}}{2}\left|P^t_{grid}\right|\right)+\left(\sum_{i\in N_{DG}} f_i\left(P^t_{G,i}\right)+C_{up,i}S^t_{up,i}+C_{dn,i}S^t_{dn,i}\right)+\sum_{i\in N_z}\left[f_{PV}\left(P^t_{PV,i}\right)+f_{wind}\left(P^t_{wind,i}\right)+f_{batt}\left(P^t_{batt,i}\right)\right]+\sum_{i\in N_C}C_{C,i}P^t_{chil,i}+\sum_{i\in N_P}C_{P,i}P^t_{pump,i}\Bigg\} \quad (1)$$

The objective is formulated in (1), where C^t_{buy} and C^t_{sell} are purchased and sold electricity prices from/to the grid at time t, respectively (shown in Fig. 3), P^t_{grid} is the grid power, $f_i(P^t_{G,i})$

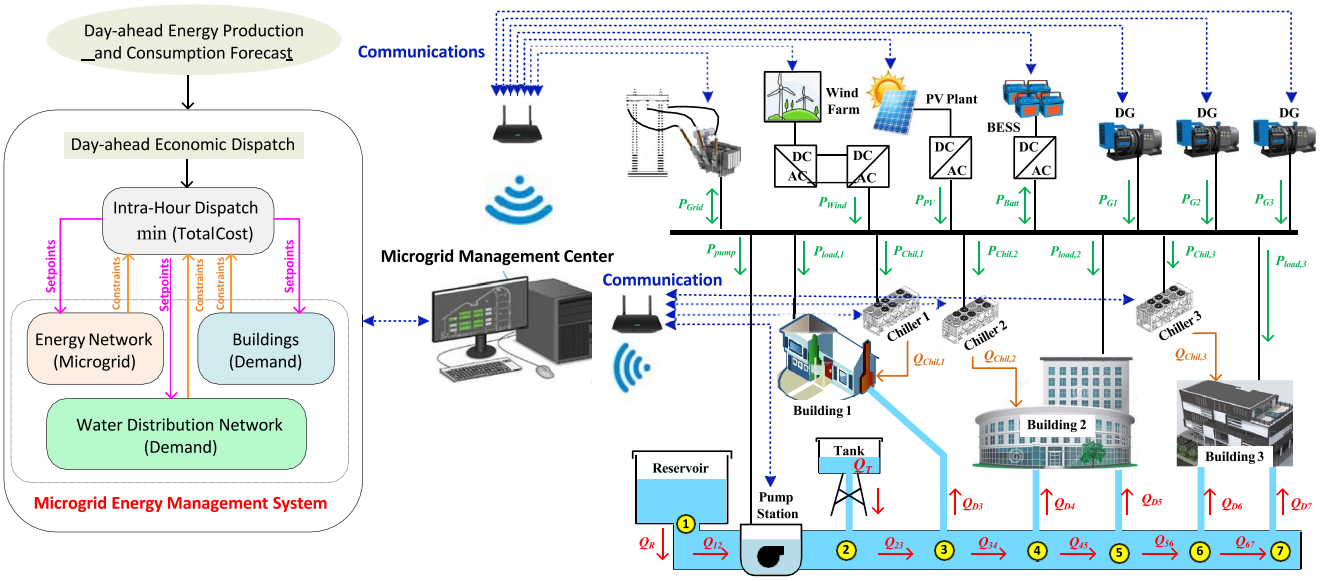

Fig. 1. Structure of the proposed energy management system for an energy-water microgrid with buildings and water distribution system.

are cost functions of conventional DG plants as a quadratic function of their generated power $P^t_{G,i}$. The absolute value $|P^t_{grid}|$ will be expanded as $P^t_{grid} \le y$ and $-P^t_{grid} \le y$ to be linearized. The term $|P^t_{grid}|$ will be replaced with y in (1), and the two new inequalities will be added to the linear inequality constraints of the MILP problem [15]. Furthermore, $C_{up,i}$ and $C_{dn,i}$ are the startup and shutdown costs, $S^t_{up,i}$ and $S^t_{dn,i}$ are the startup and shutdown status of ith DG unit at time t, f_{PV}, f_{wind}, and f_{batt} are cost functions of PV plant, wind farm, and battery energy storage units in terms of their respected output power (e.g., P^t_{PV}, P^t_{wind}, and P^t_{batt}, respectively). In addition, $\mathcal{N}_z$ is a set of buses, where $z = \{\text{PV, wind, batt}\}$. The last two components of the objective function (1) represent the operation and maintenance cost function of chillers ($C_{C,i}$ and $C_{P,i}$) in terms of their consumed powers, $P^t_{chil,i}$ and P^t_{pump}, respectively. Cost functions of DGs expressed in (1) are quadratic univariate functions in the form of $a_i(P^t_{G,i})^2 + b_i P^t_{G,i} + c_i$, where a_i, b_i, and c_i are cost coefficients of the ith generation plant. Due to the nonlinear nature of DGs' cost functions, piecewise linear approximation is used to linearize the objective function. This concept is well studied in the literature [16].

2) Load Balance Constraint: The main constraint of the economic dispatch problem is the load balance which guarantees that the optimal allocation of energy resources in (2) meets the demand.

$$P^t_{grid} + \sum_{i\in N_{DG}} P^t_{G,i} + \sum_{i\in N_{PV}} P^t_{PV,i} + \sum_{i\in N_{wind}} P^t_{wind,i} + \sum_{i\in N_{batt}} P^t_{batt,i} = \sum_{i\in N_C} P^t_{chil,i} + \sum_{i\in N_P} P^t_{pump,i} + \sum_{i\in N_l} P^t_{load,i} \tag{2}$$

where summation of generated powers from the grid, DGs, PV, wind, and BESS should be equal to the consumed power. Here, $T \in \{1, \ldots, 24\}$, N_{DG}, N_{PV}, N_{wind}, and N_{batt} represent the number of DG, PV, wind, and battery generation units. In this equation, $P^t_{chil,i}$ is the consumed power by the chiller in building i to meet the thermal demand of the building, P^t_{pump} is the power consumption of the pump in the water distribution system shown in Fig. 1 during hour t, and $P^t_{load,i}$ is the electrical load of building i during hour t. In addition, N_C is the number of chillers in the building, N_p is the number of pumps in the water distribution system, and N_l is the number of loads in ith building.

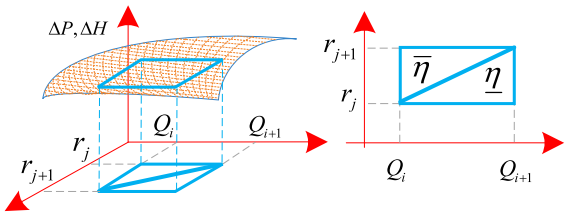

Fig. 2. Piecewise linear approximation of bivariate functions (ΔH and ΔP).

III. Energy Management of Generation Units

A. Constraints of DG Units

A unit commitment formulation in (3)-(7) is used to represent the constraints of DG units in order to minimize the total commitment cost [16]. In power limit constraint of DG units in (3), $U^t_{DG,i} \in \{0, 1\}$ is a binary variable indicating on/off status of DG unit i. Equations (4) and (5) represent the ramp up and down limits of ith DG, respectively. Also, $S^t_{up,i}$ and $S^t_{dn,i}$ in (6) and (7) are two binary variables representing start up and shut down status of ith DG unit at time t, respectively.

$$U^t_{DG,i} P^{min}_{G,i} \le P^t_{G,i} \le U^t_{DG,i} P^{max}_{G,i} \tag{3}$$

$$P^t_{G,i} - P^{t-1}_{G,i} \le R^{max}_{up} U^{t-1}_{DG,i} \tag{4}$$

$$P^{t-1}_{G,i} - P^t_{G,i} \le R^{max}_{down} U^t_{DG,i} \tag{5}$$

$$S^t_{up,i} = \text{Max}\left(0, U^t_{DG,i} - U^{t-1}_{DG,i}\right), \quad \forall i \in DG, \forall t \in T \tag{6}$$

$$S^t_{dn,i} = \text{Max}\Big(0,\, U^{t-1}_{DG,i} - U^t_{DG,i}\Big), \quad \forall i \in DG, \forall t \in T \tag{7}$$

It is noted that (6) and (7) are converted to standard linear form using the following formulation for $x = \text{Max}(a, b)$ as

$$\begin{aligned} &\min_x \ x \\ &\text{s.t. } x \geq a,\ x \geq b \\ &\quad x \leq a + Mu_x,\ x \leq b + M(1 - u_x) \end{aligned} \tag{8}$$

where $u_x \in \{0, 1\}$ is a new binary variable introduced for variable x, and M is a big number.

B. Constraints of Renewable Sources

1) Wind Generation Constraints: Constraints of the wind generation plant are expressed in the following equations.

$$f_{wind}\big(P^t_{wind,i}\big) = K_{wind,i} P^t_{wind,i} \tag{9}$$

$$P^{min}_{wind,i} \leq P^t_{wind,i} \leq P^{max}_{wind,i} \tag{10}$$

Equation (9) represents the maintenance and operation cost of wind turbines as a function of their generated power, where K_{wind} is the cost coefficient of the wind plant. Equation (10) bounds the wind energy generation to the maximum and minimum available wind power.

2) Solar Generation Constraints: Solar generation output depends on weather conditions and is highly uncertain. The proposed microgrid model shown in Fig. 1 has an aggregated PV plant and the constraints related to the operation of PV plant are formulated as

$$f_{PV}\big(P^t_{PV,i}\big) = K_{PV,i} P^t_{PV,i} \tag{11}$$

$$P^{min}_{PV,i} \leq P^t_{PV,i} \leq P^{max}_{PV,i} \tag{12}$$

where (11) represents the cost of PV generation plant at time t and K_{PV} is the cost coefficient of PV plant. The PV output power generation is also restricted to the maximum and minimum available power as enforced in (12).

C. Battery Energy Storage System Constraints

Battery energy storage system (BESS) in the economic dispatch model can provide both charging and discharging powers, therefore, the bi-directional nature of storage units should be considered. The following constraints represent the BESS constraints for the developed model

$$f_{batt}\big(P^t_{batt,i}\big) = K_{batt,i} P^t_{batt,i} \tag{13}$$

$$-P^{Max}_{chg,i} \leq P^t_{batt,i} \leq P^{Max}_{dis,i} \tag{14}$$

$$E^{t-1}_{batt} = E^t_{batt,i} + \eta_{batt,i} P^t_{batt,i} \Delta t \tag{15}$$

$$E^{Min}_{batt,i} \leq E^t_{batt,i} \leq E^{Max}_{batt,i} \tag{16}$$

where (13) relates the cost of operation of the BESS to its consumed/generated power, η_{batt} is the charging/discharging efficiency of the BESS unit, which is η for charging and $1/\eta$ for discharging, assuming charging and discharging efficiencies are similar and equal to η [17], and $K_{batt,i}$ is the purchased power coefficient of the BESS unit. Equation (14) limits the output power of the BESS unit to the maximum discharging ($P^{Max}_{dis,i}$) and maximum charging ($P^{Max}_{chg,i}$) limits. Equation (15) provides the relationship between the available energy of the BESS unit and its output power. The last constraint in (16) limits the energy of the BESS between its maximum and minimum available energy levels. In this equation, Δt is the step size of the economic dispatch problem, which is considered as 1 hour in this study. The start/end-of-day (EoD) energy limit of battery can be added to the optimization model to ensure the BESSs will have enough energy at the beginning of the next day. This constraint is enforced by [17], [18]

$$E^{t_{end}}_{batt,i} = E^{t_0}_{batt,i} \tag{17}$$

where t_{end} is the time at the EoD (i.e., at hour 24) and $E^{t_0}_{batt,i}$ is the initial energy level of BESS at the beginning of the day.

IV. Buildings Thermal Energy Management

In this paper, a summer cooling scenario is considered, which can easily be extended to other cooling/heating scenarios. Therefore, a smart thermal management system considering the thermal comfort level of occupants is considered to intelligently manage the cooling devices and reduce the operational costs. The cooling demand depends on the temperature forecast over a 24-hour period and customer temperature comfort range of buildings due to their heat storage capability.

1) *Nonlinear Thermal Management:* The optimization model will include a thermal management subsystem, where a system of nonlinear equations associated with heat transfer processes are added to the economic dispatch.

$$\begin{aligned} \rho C V_k \frac{d\Delta T^t_{in,k}}{dt} = \sum_{k \in N_B} \big\{ & Q^t_{wall,k} + Q^t_{win,k} + Q^t_{in,k} \\ & + Q^t_{wall,solar,k} + Q^t_{win,solar,k} - Q^t_{chil,k} \big\} \end{aligned} \tag{18}$$

$$Q^t_{wall,k} = \sum_{j \in N_{wall}} U_{wall,j} A_{wall,j} \big(T^t_{out} - T^t_{in,k}\big) \tag{19}$$

$$Q^t_{win,k} = \sum_{j \in N_{win}} U_{win,j} A_{win,j} \big(T^t_{out} - T^t_{in,k}\big) \tag{20}$$

$$Q^t_{wall,solar,k} = \sum_{p \in \mathcal{D}} \sum_{j \in N_{wall}} a_{wall,j} R_{wall,j} U_{wall,j} I^t_{r,p} \tag{21}$$

$$Q^t_{win,solar,k} = \sum_{p \in \mathcal{D}} \sum_{j \in N_{win}} \alpha_{win,j} \beta_{win,j} I^t_{r,p} \tag{22}$$

The thermal management system in the economic dispatch problem will solve a first order partial differential equation to keep the indoor temperature of the buildings within the comfort level of customers (20-25°C referring to [19]) during the occupancy hours. A case is also considered, where fixed temperature settings are used throughout a day regardless of occupancy. Thermal management constraints of the building sector in the proposed economic dispatch model are presented in equations (18)-(22). Building's thermal equilibrium formula in (18) relates the indoor temperature and outdoor temperature forecast to the cooling demand identified by the chillers. In this equation, ρ, C, and V_k are the heat density in kg/m^3, heat capacity in $\frac{J}{kg°C}$, and volume of air in m^3 in the building number $k \in N_B = \{1, 2, 3\}$. Moreover, T^t_{in} is the indoor

temperature, which is controlled by the chiller, and T^t_{out} is the outdoor temperature, which is the result of temperature forecast for 24 hours.

In equation (18), $Q^t_{wall,k}$ and $Q^t_{win,k}$ are overall heat gains of walls and windows in building k in kW, which are derived based on (19) and (20). In addition, $Q^t_{in,k}$ in kW is the internal heat gain of building k due to occupancy or heat gains of appliances, $Q^t_{wall,solar,k}$ and $Q^t_{win,solar,k}$ are the heat gains of walls and windows in building k due to solar radiation, respectively, which are derived based on (21) and (22). Contributions from solar radiation on the surface of external walls ($Q^t_{wall,solar,k}$) and windows ($Q^t_{win,solar,k}$) in different directions, $\mathcal{D} \in \{$north, east, west, and south$\}$ are considered. The negative sign of chiller's cooling gain, $Q^t_{chil,k}$, in (18) denotes the cooling power of chillers to regulate the indoor temperature. On the right side of (18), $Q^t_{wall,k}$ is the heat transfer (in kW) through the external walls in the building, which is the sum of contributions of individual external walls, N_{wall} is the number of walls in different orientation j in building number P, $A_{wall,j}$ is the area in m^2 for the j^{th} wall, T^t_{out} is the output temperature at time t and T^t_{in} is the indoor temperature at time t. In addition, in (19)-(22), $U_{wall,j}$ and $U_{win,j}$ are the heat transfer coefficients of the walls and windows, respectively, $A_{wall,j}$ and $A_{win,j}$ are the wall and window areas in m^2 for the j^{th} wall and window, respectively. The heat contributions to the volume's walls and windows through solar radiation is calculated according to the ISO 13790 standard [19], where $\alpha_{wall,j}$ is the absorbance coefficient of wall external surface, $R_{wall,j}$ is the resistance of the external wall against radiation, $I^t_{r,p}$ is the solar radiation to the external wall in orientation p, $\alpha_{win,j}$ is the glass transmission coefficient of windows and $\beta_{win,j}$ is the shading coefficient of the windows. The internal heat gain in each building is calculated by adding the internal heat gains of people, appliances, and lighting referring to [20].

2) *Linearization of Nonlinear Heat Equilibrium Function:* The thermal equilibrium formula in (18) is a nonlinear heat flow due to the presence of the derivative term, therefore, to convert the equilibrium formula to a standard linear form, the differential equation is converted to a finite difference equation with a forward difference approximation on the time derivative. More information on conversion of heat flow equilibrium to a steady flow using difference approximation can be found in [21].

$$\rho C V_k\left(T^{t+1}_{in,k} - T^t_{in,k}\right) = \Delta t\left[\sum_{k\in N_B}\left\{Q^t_{wall,k} + Q^t_{win,k} + Q^t_{in,k} + Q^t_{wall,solar,k} + Q^t_{win,solar,k} - Q^t_{chil,k}\right\}\right] \quad (23)$$

In (23), the variables to be solved by the economic dispatch problem are T^{t+1}_{in}, which is the temperature setpoint (T_{set}) for the next hour of operation, and the power consumption of chiller for the current hour $P^t_{chil,k} = \frac{Q^t_{chil,k}}{\varsigma_k}$, where ς_k is the energy efficiency coefficient of the electric chiller.

V. Water Demand Management

1) *Constraints of Water Distribution System:* The water demand management model minimizes the electricity consumption of pumps, as the most energy intensive elements in water distribution networks, while the hydraulic demands are met at all the nodes. Constraints of water distribution system are expressed in the following

Equation (24) relates the water flow of ith pump, which is installed between nodes m and n to the flow of pipe, $Q^t_{m,n}$. In this equation, S^t_i is a binary variable representing the status of the pump, Δh_i is the head gain, and B is the specific weight of water at 20°C.

Equation (25) relates the head gain to the water flow in the pipe associated to the pump (pipe connecting node m to node n) and normalized pump speed, r_i, where a_p, b_p, and c_p are coefficients of the pump characteristics.

$$P^t_{pump,i} = S^t_i B Q^t_{m,n}\Delta h^t_i,\ \ S^t_i \in \{0,1\} \quad (24)$$

$$\Delta h^t_i = a_{p,i}\left(Q^t_{m,n}\right)^2 + b_{p,i}Q^t_{m,n}r^t_i + c_{p,i}\left(r^t_i\right)^2 \quad (25)$$

$$\left\{\sum_{i,j\in N_w} A_{ij}.{q_j}^t\right\} - Q^t_R + Q^t_T = -Q^t_D + Q^{t-1}_T \quad (26)$$

$$\begin{cases} S^t_i = 1 & \text{if } Q^0_T + Q^t_T < Q^{min}_T \\ S^t_i = 0 & \text{if } Q^0_T + Q^t_T > Q^{max}_T \end{cases} \quad (27)$$

$$H^t_m - H^t_n + \left(Z^t_m - Z^t_n\right) + \Delta h^t_i = F_{m,n}\left(Q^t_{m,n}\right)^{1.85} \quad (28)$$

Equation (26) expresses the conservation of mass theorem such that at any hour, the amount of water supplied by the reservoir should be equal to water accumulated in the tank, consumed (by customers), and flowed in the pipes. In (26), Q^t_R is the flow injected to the pipe at time t from the reservoir in m^3/h, Q^t_T is the flow in the tank in m^3/h at time t, Q^t_D is the total water demand in m^3/h at time t which is equal to the summation of water usage at each node, and A_{ij} is the incident matrix of the water network with nodes and pipes associated with the rows and columns of the matrix, respectively. Each element $a_{i,j}$ (corresponding to node i and flow passing through pipe j) belongs to the subset $\{1, -1, 0\}$, where 1 or -1 are assigned to $a_{i,j}$ when flow j enters or exits the node j, respectively, while $a_{i,j}$ is 0 if flow j is irrelevant to the node i. Here, $\mathbf{q}$ is the vector of pipes' flow rates, where q_j is associated with the flow rate of pipe j [22].

Equation (27) controls the status of the pump connected to the tank within the minimum amount required to supply the network for one day (Q^{min}_T) and the maximum amount allowed to avoid overflowing the tank (Q^{max}_T) considering the initial water level in a tank, Q^0_T.

Equation (28) is the Bernoulli's theorem stating the difference between the energy head of any two nodes is equal to the gained energy (dissipated by the pump) minus the amount lost in the form of head loss [22]. In equation (28), H_m and H_n represent the pressure head of nodes m and n, Z_m and Z_n are the elevations at nodes m and n in meters. In addition, $F_{m,n}$ is the head loss of a pipe connecting node m to node n, and can be computed by $F_{m,n} = {L_{m,n}}/{(0.278CD^{2.63}_{m,n})^{1.85}}$, where $L_{m,n}$ and $D_{m,n}$ are the length and diameter of the pipe connecting nodes m and n, respectively, and C is the friction factor of the

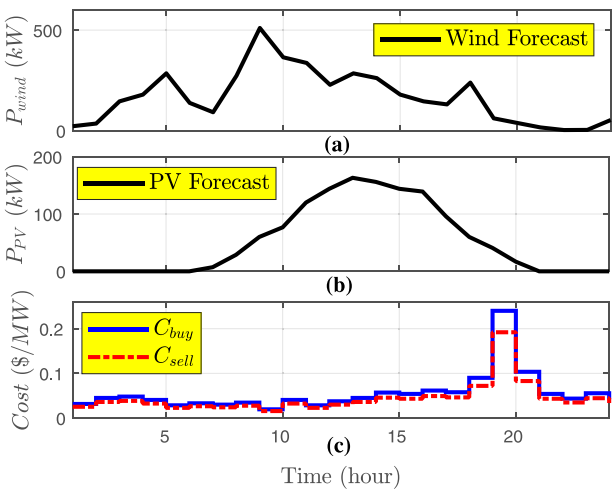

Fig. 3. (a) PV and (b) wind forecast data and (c) electricity prices.

pipe. The start/EoD water level of the tank can also be added to ensure the tank will have sufficient amount of water at the beginning of the next day:

$$Q_T^{t_{end}} = Q_T^{t_0} \tag{29}$$

where t_{end} is the time at the EoD (hour 24) and $Q_T^{t_0}$ is the initial water level of the tank at the beginning hour of the day.

2) *Linear Approximation of Nonlinear Functions:* Since the pump's output power in (24) and Bernoulli's equation in (28) are inherently bivariate nonlinear functions, they should be approximated by their linear approximate functions. Therefore, piecewise linear approximation of bivariate functions is used. Let us define $\mathcal{P}$ and $\mathcal{H}$ as two bivariate functions representing pump's output power and head gain,

$$\mathcal{P}\big(Q_{m,n}^t, r_i^t\big) = BQ_{m,n}^t \Delta h_i^t \tag{30}$$

$$\mathcal{H}\big(Q_{m,n}^t, r_i^t\big) = F_{m,n}\big(Q_{m,n}^t\big)^{1.85} - \Delta h_i^t \tag{31}$$

The piecewise linearization of $\mathcal{P}$ and $\mathcal{H}$ is illustrated in Fig. 2, where ξ sampling coordinates on Q-axis and τ sampling coordinates on r axis can be considered. The functions $\mathcal{P}$ and $\mathcal{H}$ are evaluated for each breakpoint $(Q_i, r_j)(i = 1, \ldots, \xi, j = 1, \ldots, \tau)$. For any given point $(\bar{Q}, \bar{r})$ with $Q_i \le \bar{Q} \le Q_{i+1}$ and $r_j \le \bar{r} \le r_{j+1}$, a rectangle of vertices (Q_i, r_j), (Q_{i+1}, r_j), (Q_i, r_{j+1}), and (Q_{i+1}, r_{j+1}) is considered (see Fig. 2). By drawing a diagonal of this rectangle, two triangles known as upper and lower triangles are formed (see the right-side plot on Figure 2).

The lower triangle is differentiated by a binary variable $\underline{\eta}$ and the upper triangle is differentiated by $\bar{\eta}$. The function value at $(\bar{Q}, \bar{r})$ is approximated using a convex combination of the function values evaluated at the vertices of the triangle containing $(\bar{Q}, \bar{r})$. By replacing Δh_i^k from (25) in (30), the non-linear bivariate function of pump power is found

$$\mathcal{P} = BQ_{m,n}^t\Big[a_{p,i}\big(Q_{m,n}^t\big)^2 + b_{p,i}Q_{m,n}^t r_i^t + c_{p,i}(r_i^t)^2\Big] \tag{32}$$

The pump's output power can then be expressed by $P_{pump,i}^t = S_i^t\mathcal{P}$, which is a non-linear combination of pump's bivariate function $\mathcal{P}(Q_{m,n}^t, r_i^t)$ and binary variable S_i, which is converted to a standard linear programming formulation using Big M method

$$-MS_i^t \le \mathcal{P} \le MS_i^t \tag{33}$$

$$P_{pump,i}^t - M\big(1 - S_i^t\big) \le \mathcal{P} \le P_{pump,i}^t + M\big(1 - S_i^t\big) \tag{34}$$

Next, referring to (28), define $\mathcal{H}(Q_{m,n}^t, r_i^t) = H_m^t - H_n^t + (Z_m^t - Z_n^t)$ as a bivariate function representing the Bernoulli's equation, therefore,

$$\mathcal{H}\big(Q_{m,n}^t, r_i^t\big) = F_{m,n}\big(Q_{m,n}^t\big)^{1.85} - \Delta h_i^t \tag{35}$$

Substituting Δh_i^t from (25) in (35),

$$\mathcal{H} = F_{m,n}\big(Q_{m,n}^t\big)^{1.85} - a_{p,i}\big(Q_{m,n}^t\big)^2 - b_{p,i}Q_{m,n}^t r_i^t - c_{p,i}\big(r_i^t\big)^2 \tag{36}$$

Equations (32) and (36) are two bivariate functions that are approximated by piecewise linearization technique by dividing the Q-axis into ξ segments and finding associated $Q_{m,n}^t$ for the breakpoints $(Q_{b,i})$, dividing the r-axis into τ segments and finding associated r_i^t for the breakpoints $(r_{b,j})$, introducing $\xi \times \tau$ continuous variables $\alpha_{i,j} \in [0, 1]$, and extending the equations to a three-dimensional space such that

$$Q_{m,n}^t = \sum_{i=1}^{\xi}\sum_{j=1}^{\tau}\alpha_{i,j}Q_{b,i} \tag{37}$$

$$r_i^t = \sum_{i=1}^{\xi}\sum_{j=1}^{\tau}\alpha_{i,j}r_{b,j}, \quad \sum_{i=1}^{\xi}\sum_{j=1}^{\tau}\alpha_{i,j} = 1 \tag{38}$$

$$\mathcal{H}\big(Q_{m,n}^t, r_i^t\big) = \sum_{i=1}^{\xi}\sum_{j=1}^{\tau}\alpha_{i,j}\mathcal{H}\big(Q_{b,i}, r_{b,j}\big) \tag{39}$$

$$\mathcal{P}\big(Q_{m,n}^t, r_i^t\big) = \sum_{i=1}^{\xi}\sum_{j=1}^{\tau}\alpha_{i,j}\mathcal{P}\big(Q_{b,i}, r_{b,j}\big) \tag{40}$$

$$\sum_{i=1}^{\xi-1}\sum_{j=1}^{\tau-1}\Big(\bar{\gamma}_{i,j} + \underline{\gamma}_{ij}\Big) = 1, \ \ \bar{\gamma}_{i,j}, \underline{\gamma}_{ij} \in \{0, 1\} \tag{41}$$

$$\alpha_{ij} \le \bar{\gamma}_{i,j} + \underline{\gamma}_{i,j} + \bar{\gamma}_{i,j-1} + \underline{\gamma}_{i-1,j-1} + \bar{\gamma}_{i-1,j-1} + \underline{\gamma}_{i-1,j} \tag{42}$$

Constraints (37) and (38) represent the liner approximation of flows and pump speeds, respectively and there exists only two consecutive α with nonzero values. Constraints (39) and (40) denote the linear approximation of $\mathcal{H}$ and $\mathcal{P}$, respectively. Constraint (41) enforces that any given solution will be located in only one triangle (upper or lower) for the convex combination. Furthermore, (42) imposes that only non-zero α_{ij} values are the ones associated with three vertices of the triangle chosen in (41). Therefore, Equations (37)-(42) are linear approximation of (24), (25), and (28). Finally, equation (27), which represented the non-linear behavior of tank level, can be linearized using the big M method as the following

$$Q_{min}^T - MS_i^t < Q_0^T + Q_T^t < Q_{max}^T + M\big(1 - S_i^t\big) \tag{43}$$

The above linear approximates will represent the water distribution system constraints in the economic dispatch model.

Algorithm 1 Water-Energy-Building Economic Dispatch

Input Data Electricity price, PV and wind forecast data
Input Data 24-hour temperature, load, and solar radiation forecast, building occupancy hours, and water demand
Procedure Economic Dispatch **then**
  for $t \in T$ **do**
    for $\forall\ \mathcal{N}_{DG}, \mathcal{N}_{PV}, \mathcal{N}_{wind}, \mathcal{N}_{batt}, \mathcal{N}_{C}, \mathcal{N}_{P}$ **do**
      Minimize total cost referring to (1)
      Ensure load balance is met referring to (2)
      Ensure targeted line flow exceeds maximum flow, F_k^{max}
      Run the unit-commitment problem, referring to (3)-(5) & (8)
      Ensure powers of all the DGs, renewables, and loads are bounded
      Run the energy management constraints of BESSs referring to (14)-(16)
      Run the energy management of buildings refer -ring to (19)-(22) & (23)
      Run the water management formulation referr -ing to (26)-(28) & (37)-(43)
    end for
  end for
  return 24-hour dispatch of generation units, pumps, and chillers

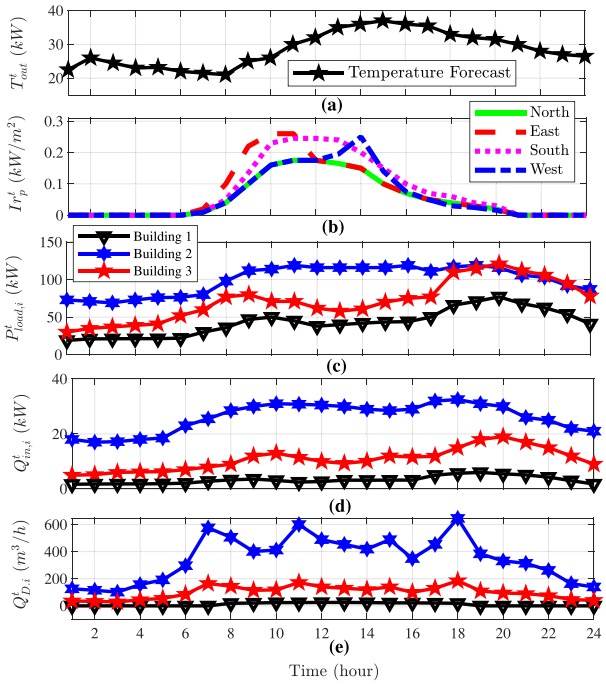

Fig. 4. The 24-hour profile of (a) temperature forecast, (b) solar radiation forecast, (c) electrical load forecast, (d) internal heat gains of buildings, and (e) water demand.

Therefore, the proposed optimization model for the energy-water smart grid system is represented as a mixed integer linear programming problem and a global optimum can be guaranteed for this system.

3) *Algorithm of the Proposed Economic Dispatch Model:* The algorithm of the proposed integrated economic dispatch is shown in Algorithm 1. As it can be seen, the proposed energy management formulation receives input data on electricity price, PV, and wind forecast data, temperature, and solar radiation data over 24 hours. In addition, the water demand, comfort level settings in the buildings, and load of the buildings will be supplemented to the program as inputs. The economic dispatch problem will then be formulated to minimize the overall cost of the combined water-energy-building system considering constraints of each sector (energy, water, and building). The outputs of the proposed energy management will be 24-hour dispatch of generation units in microgrid, optimal power consumption of pumps to meet the daily water demand, and optimal consumption of chillers to meet the thermal demand of the buildings.

VI. Case Studies

The proposed MILP formulation is solved using "SCIP" linear solver of MATLAB in OPTI Toolbox, which is an open-source MATLAB toolbox [23]. The "SCIP" solver is reported as the fastest non-commercial mixed integer programming solver that also solves non-convex problems to global optimality [24]. All optimization models were run on a processor of Intel Core CPU i9-9900K at 3.6GHz and 32GB RAM.

As the proposed formulation is a standard linear programming problem, it can be easily expanded for large-scale microgrids. However, for large-scale microgrids, the number of variables and constraints will significantly increase due to piecewise linearization, which may reduce the computational efficiency of the proposed solution. The system under investigation is illustrated in Fig. 1, where parameters of the microgrid model and water distribution system are listed in [13], and the DG and building parameters are adopted from [20]. The 24-hour forecasts for temperature and solar radiation on different directions adopted in the case studies are illustrated in Fig. 4(a) and Fig. 4(b), respectively. The diurnal wind and solar power generation forecasts for the case studies are also shown in Fig. 3(a) and Fig. 3(b), respectively. The maximum available wind and PV output powers are obtained based on the wind speed and weather forecast for 24 hours. In addition to the microgrid, three different types of building are considered in this study serving as the end-users of the water and energy sources, as depicted in Fig. 1. The occupancy hours of these buildings are listed in the following

- Building 1 (Residential) is occupied from 7:00 p.m. till 9:00 a.m.,
- Building 2 (Office) is occupied from 9:00 a.m. to 9:00 p.m.,
- Building 3 (Apartment) is occupied 24 hours.

The electrical and water demand forecasts of the buildings, $P^t_{load,i}$, for the 24 hours of operation are illustrated in Fig. 4(c) and 4(e), respectively. Moreover, the 24-hour internal heat gains of four buildings in the studied system during a summer day is illustrated in Fig. 4(d). The case studies are aimed to investigate the effects of thermal energy and water demand response management of the targeted buildings on the energy generation and economic dispatch of the microgrid system. It is noted that the start/EoD energy limit of battery is only considered for Case 1.

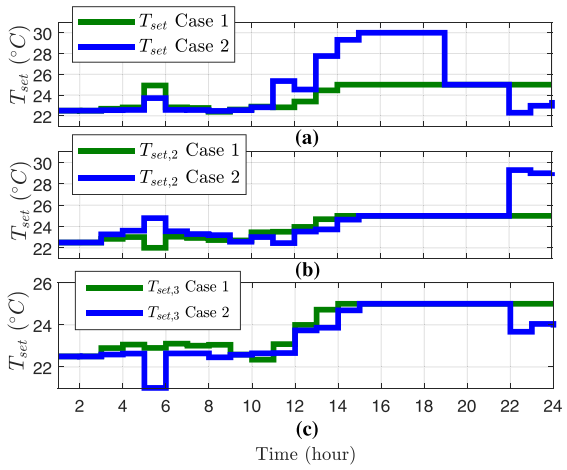

Fig. 5. Indoor temperature settings during 24 hours for (a) building 1, (b) building 2, and (c) building 3, for cases 1 and 2.

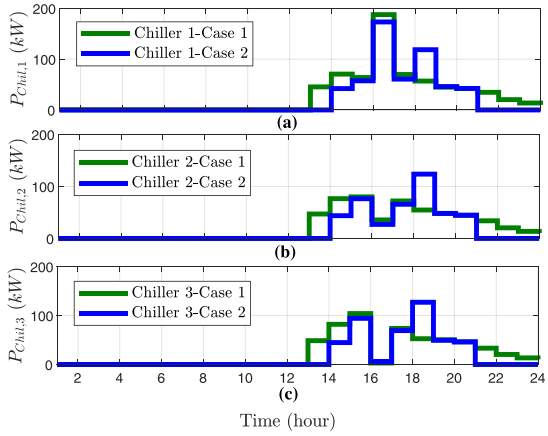

Fig. 6. Power consumption of chillers during 24 hours for cases 1 and 2 for (a) building 1, (b) building 2, and (c) building 3.

1) *Case 1:* This case investigates the impact of thermal management system on the day-ahead economic dispatch of the system. Two scenarios are considered; (a) without EoD energy limit of battery in (17) and (b) with EoD energy constraint of battery. The temperature settings of the buildings are set to 20-25°C during the day regardless of occupancy. Therefore, the chillers in the buildings operate in order to keep the indoor temperature within the scheduled comfort level of occupants during the day. Results are illustrated in Fig. 5, where the temperature setpoints of individual buildings for case 1 are shown with green color. It is observed that the temperature setting for all the buildings is within 20 to 25°C during the entire operation time.

The power consumption of chillers for the three buildings in this case is illustrated by green color in Fig. 6. It is observed that chillers only operate if there is a significant mismatch between the outdoor temperature and indoor temperature (e.g., hours 13-24 referring to Fig. 5).

Contribution of generation units to the overall load of the microgrid system is illustrated in Fig. 7, where Fig. 7(a) is the economic dispatch without EoD battery constraint, and

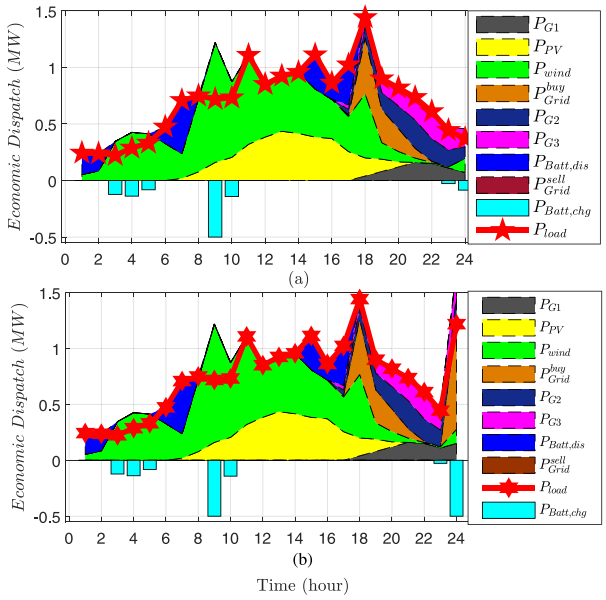

Fig. 7. Economic dispatch of the system for case 1, (a) without EoD energy limit for storage, (b) with EoD energy limit for storage.

Fig. 7(b) forces the EoD energy limit of the storage unit to be equal to the initial energy level. As it can be seen, a peak occurred during hour 24 in Fig. 7(b) to charge the battery. It is observed that the total electric power load consisting of the total demand of water distribution system, total demand of the chillers, and electricity demand of the buildings (red color line) is mainly covered by BESS and wind generation, while the surplus energy is used to charge the battery during hours 3-5 and 9-10. The DG units are shut down in the first 16 hours of operation and they start up when the peak of electricity consumption occurs during hours 17-22.

2) *Case 2:* In the second case, the impact of customer's comfort level during occupancy hours on economic dispatch of the microgrid system is studied. In this scenario, the temperature settings of buildings are kept within the standard comfort level of 20-25°C during occupancy for all the buildings. The temperature setting of building 3 during unoccupied hours is to 20-25°C. The settings for the unoccupied hours of Building 1 and 2, however, have been modified to stay within 15-30°C. Temperature setpoint results are shown in Fig. 5 with blue color line. Compared to case 1, it is observed that the setpoint of Building 1 has been set to 30°C between hours 15-19 (unoccupied hours) to reduce the power consumption of the chiller, while the setting was at 25°C for case 1. Similar pattern can be observed for Building 2 in hours 3 and 22-24 to ensure the lowest cost.

By taking a look at the chillers' power consumption in case 2 (shown by blue color line in Fig. 6), it is observed that power consumption of chillers between hours 13-17 and 21-24 has significantly reduced for all buildings. It is also noted that in Case 2, the temperature setting of building 1 in hour 19 is reduced by 5 degrees, compared to hour 18, (see Fig. 5), which resulted in a significant peak on power consumption of chiller for building 1 during hour 18 (see first subplot in Fig. 6). This justifies the fact that chiller will be started ahead

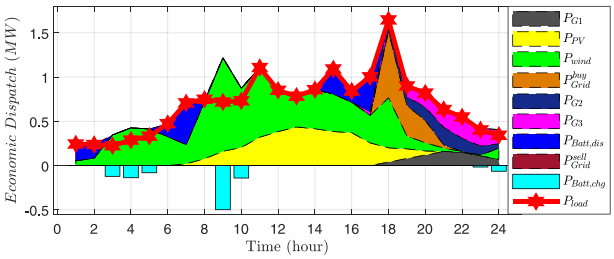

Fig. 8. Economic dispatch of the system for case 2.

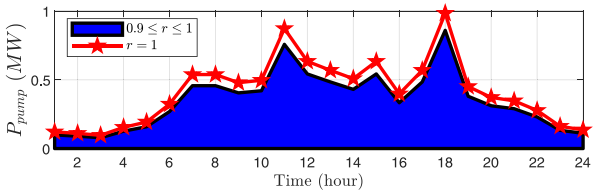

Fig. 9. Effect of pump's speed on daily power consumption of water distribution network.

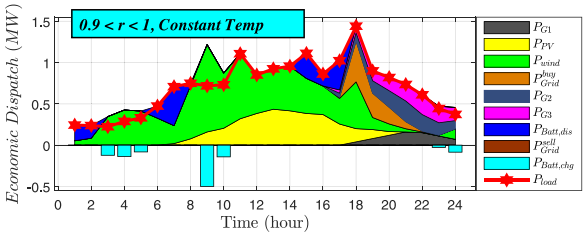

Fig. 10. Effect of pump's speed on economic dispatch, with constant temperature settings of 20-25°C over 24 hours.

of time to keep the temperature of the building 1 within the comfort level range for the next hour.

By taking a look at the economic dispatch of the system for case 2 (shown in Fig. 8), it is observed that power consumption has been reduced during hours 13-17 and 21-24 as expected due to the reduction of power consumption of chillers. However, large peak demand is enforced in this case during hour 18, which has increased the total demand to almost 1.7MW, which is 200kW more compared to case 1.

3) *Case 3:* In this case study, the effect of pump's speed on the economic operation of the system is considered. Herein, a variable-speed for the pump's motor drive is contemplated such that $0.9 \leq r \leq 1$, for buildings with 24-hour temperature settings (similar to Case 1). The economic dispatch runs the optimization problem considering that the pump's speed is adjustable depending on the hour-ahead water demand forecast and the water level in the tank during the 24-hour operation. The power consumption of the pump in the water distribution system during the 24-hour operation is illustrated in Fig. 9. It is observed that the power consumption of water distribution system is significantly reduced when a variable-speed pump with flexible speed settings is contemplated.

The economic dispatch of the system is illustrated in Fig. 10. It is observed that, compared to the first case study, the overall power consumption and peak demands are lower when

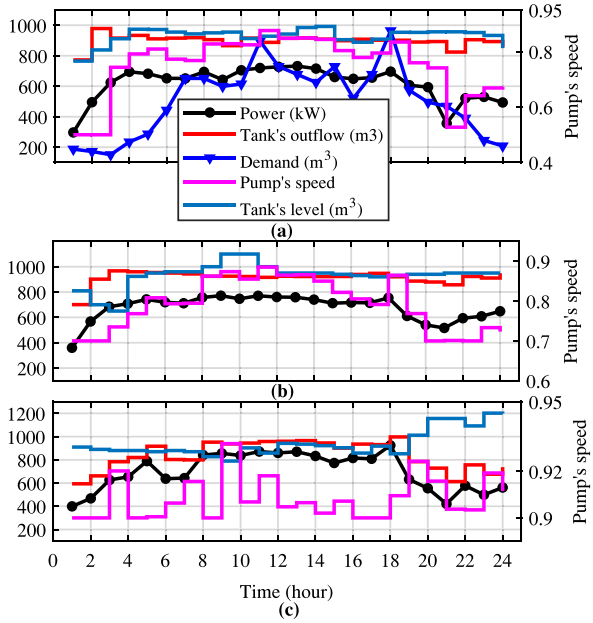

Fig. 11. Correlation between pump's speed, tank's level and outflow, demand, and pump's power consumption in buildings with temperature settings of 20-25°C in (a) $0.5 < r < 1$, (b) $0.7 < r < 1$, and (c) $0.9 < r < 1$.

variable-speed pumps are incorporated into the economic dispatch problems.

4) *Case 4:* The objective of this case study is to investigate the correlation between the hourly state of the tank (water level in the tank and its effluent), water demand, the pump's speed, and the power consumption by the pump. Also, it is curious to examine if the studied system in Case 3 can be optimized even further. As such, the system is optimized considering three scenarios, where the pump's speed is varied within three different ranges. The lowest speed is considered to be 0.5p.u., assuming the pump operates at a 50% or better efficiency [25].

Results are demonstrated in Fig. 11, where subplot (a) associates with the range of $[0.5-1]$, (b) corresponds to the range of $[0.7-1]$, and (c) is related to the to the range of $[0.9-1]$ within which the pump's speed varies. Demand profile is identical for all figures, hence it is only shown in subplot (a). Speed of the pump affects the energy consumption of the pump via (24) and (25). Also, because the pump is installed on the upstream flow of the tank, its operation is directly correlated with the water level in the tank, as well as the hourly demand of the network and the amount of water flowing through the pipes in the water network, collectively driving the tank's outflow at every hour. As can be seen in the figures, the larger the interval and the smaller the lower level of the speed are, the smoother the tank's outflow and water level (red and cyan color lines, respectively) and power consumption (black color line) graphs are appeared. Such will offset the electric peak charges and optimize the water demand response. It is noted that the tank's level at hour 24 is relaxed, not forced by an EoD constraint, and is decided by the optimization problem. As such, the water level in the tank at the beginning of each day can be different from the day before. In addition, the hourly power consumption of the pump varies with the pump's

TABLE I
DAILY COST INCLUDING PEAK DEMAND CHARGES AND TOTAL POWER CONSUMPTION OF CHILLERS AND WATER SYSTEMS

Case	1(a)	1(b)	1(c)	2	3	4
Cost ($/day)	535.98	632.8	633.19	569.8	475.7	316.6
P_{tot} (MW)	11.17	11.62	12.13	11.37	10.18	8.86

speed, agreeing with (25), decreasing as the speed decreases and vice versa. Furthermore, the hourly trend of the pump's speed emulates the water demand's profile, increasing during the peak demand and decreasing when water demand is decreased. When water usage rises, the water in the tank is consumed more rapidly and the pump must operate at a higher speed to compensate the low level of water in the tank, agreeing with (26). This is also verified by the correlation between magenta and red graphs depicted in Fig. 11. For instance in Fig. 11(a) and (b), within the first 3 hours that water demand is low, pump's speed is set to its minimum of 0.5 and 0.7 p.u., respectively, while water level in the tank slowly increases. As the water demand increases from hours 7 to 10 and the tank's water level drops, which requires more water to be supplied by the reservoir to the tank, the pump's speed increases. At hour 11, the first peak demand occurs which increases the pump's speed to 0.9 and 0.89 in (a) and (b), respectively. For the remaining hours, except at hour 18 which the second peak demand appears and that increases the pump's speed again to 0.82 (in (a)) and 0.88 (in (b)), the pump's speed decreases and so does the pump's power consumption. The same correlation exists in Fig. 11(c), but since the pump's speed changes within a narrower interval, more fluctuations are observed in both the tank's effluent and the pump's speed. The tank's outflow emulates the demand pattern more vividly when the pump's speed changes in a narrower threshold (in (c)), but it is smoother in (a) and (b). This is due to the pseudo steady-state condition of the tank in (c), as its inflow is almost at a steady rate (courtesy to the pump operating at high speed 0.9-1 p.u.). Also, such steadiness results in filling the tank up to approximately its maximum capacity at hour 24 in (c) in response to the drop in water consumption at the final hours of the day.

5) *Cost Analysis:* A comparison between the daily electricity costs of four case studies are shown in Table I. Considering Case 2, where the pump's actual speed is constant over the 24-hour period of operation, and equivalent to its nominal speed, the daily cost of energy generation is $33.82 more than the daily cost calculated for buildings with temperature settings fixated at the comfort level of 20-25°C over 24 hours (in Case 1(a)). Additionally, the total power consumption (P_{tot}) in Case 2 is 200kW more than that in Case 1(a). The higher cost and power consumption is due to the difference in temperature settings between the unoccupied hours and the comfort level, maintained during the occupied hours. Chillers in Case 2 must operate at higher capacity starting an hour ahead of the occupied hours to close the gap between the current indoor temperatures and the comfort level temperature settings.

The peaks occurring in Case 2 will incur additional charges to the original electric base, too. Also, the numerical results suggest that the optimization model contemplating an adjustable speed for the pump based on the water demand and tank's water level (in Case 3) reduced the daily cost more than $60 and the daily power consummation by 999kW compared to the same system with constant speed (in Case 1(a)). In Case 4 with the optimal range of 0.5 to 1 for the pump's speed, the total cost was $159 per day lower, and the total power consumption was 1.32MW lower compared to the Case 3 with the range of 0.9 to 1 for the pump's speed. This significant cost and power consumption offsetting highlights the considerable effect of optimizing pump's scheduling and operations based on the hourly water demand of the buildings, which also optimizes the tank's scheduling accordingly. By comparing Case 1(a) and Case 1(b), it is concluded that incorporation of EoD energy limit of battery storage resulted in almost $97 more daily cost and 450 kW load increase. Case 1(c) shows the impact of contemplating EoD constraints for both battery storage system and tank's level, exhibiting $0.39 and 0.51MW increase in the daily cost and power consumption over 1(b). In this scenario, states of the battery system and the tank by the end of the day are forced to be equal to their maximum capacity.

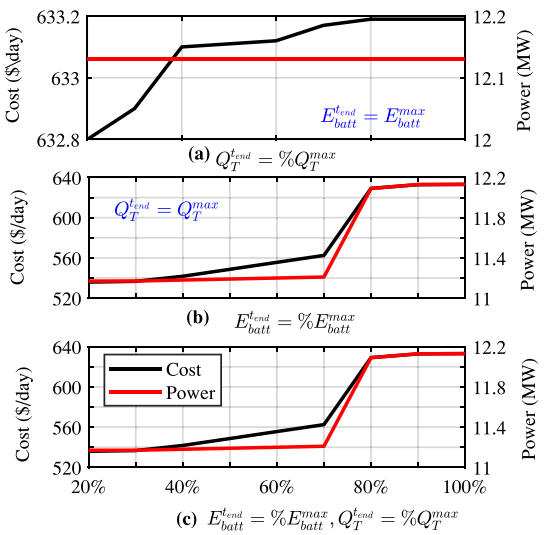

Fig. 12. Impact of contemplating EoD constraints for battery's energy and tank's level states on operational cost and total power demand of the system.

6) *Impact of EoD Constraints:* In this subsection, the EoD constraint values for the tank's level and battery storage system are optimized based on their impacts on the operational cost and total power consumption of the system. (To allow for a fair comparison, these scenarios are performed for the system described in Case 1 so that the results can be evaluated against those reported as 1(a), 1(b), and 1(c) in Table I.) As exhibited in Fig. 12, three scenarios are investigated: (a) battery storage is fully charged by the end of the day, while EoD value of the tank varies from 20% to 100% of Q_T^{max}; (b) tank is filled up to maximum capacity, while EoD value of the battery varies from 20% to 100% of E_{batt}^{max}; and (c) the EoD values for both battery and tank are varied within 20% to 100% of their maximum capacity. Results in Fig. 12(a) indicate that the EoD value of the tank had little effect on the total daily cost, ranging from $632.8 to $633.19 and total power consumption,

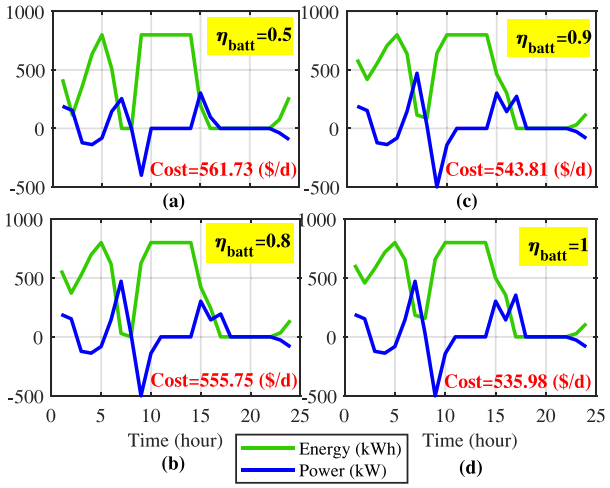

Fig. 13. Impact of battery's efficiency on the output power and energy of the battery storage system, as well as daily cost of operation.

equal to 12.13 MW. This is a reasonable result because the pump operates at nominal speed in Case 1, and because the demand decreases after 9PM, the water in the tank reaches close to its maximum capacity by the end of the day. Thus, for EoD values below that level (e.g., EoD = 20%-70%), the tank will be forced to discharge at hour 24, which would not impose an additional cost or power to the system. Because of small changes on cost incurred by varied $Q_T^{t_{end}}$, the graphs in Fig. 12(b) and (c) appear to be identical. However, total cost and power increased from \$538.97 and 11.17MW to \$633.19 and 12.13MW, respectively, as the EoD value of the battery storage system was increased from 20% to 100% of its maximum capacity. Especially, cost and power increased when EoD was set to more than 70% of its maximum capacity, which is due to the increasing utilization of fossil-fuel-based energy sources in order to charge the battery storage units, corresponding to a higher cost in the economic dispatch model. Accordingly, $E_{batt}^{t_{end}} = 0.7E_{batt}^{max}$ and $Q_T^{t_{end}} = 0.9Q_T^{max}$ are indicated as the optimal EoD values for the battery storage and tank, respectively.

7) *Impact of Battery's Efficiency:* In this scenario, the battery's efficiency is modified from 50% to 100% in Case 1 to analyze the impact of battery's efficiency on power consumption and daily cost of the system. It can be seen in the Fig. 13 (a)-(d) that as the efficiency increases from 50% to 100%, the cost of operation decreases. This is consistent with the hourly output power and energy of the battery presented with blue and green color lines, where the daily output power of the battery with lower efficiency (e.g., Fig. 13 (a)) is lower than that with higher efficiency (e.g., Fig. 13 (d)). This is damaging to the system especially during the peak demand at dark or dim hours of the day, where the combination of solar, wind, and battery energy are not enough to meet the required electrical demand of the system and thus conventional energy resources (which attribute to a higher cost in the economic dispatch model) are used to generate electricity.

8) *Discussion:* The results also agree with the findings of previous studies demonstrating that pumps are the most energy intensive devices in water distribution networks, which also affect the energy source allocation of the economic dispatch [13]. The findings demonstrated that the hourly power consumption of the chillers during the unoccupied hours in buildings with the flexible temperature settings (Case 2) is smaller than that in buildings with a 24-hour constant indoor temperature settings of 20-25°C (Case 1(a)). On the contrary during the occupied hours, the power consumption of the chillers in buildings with the flexible temperature settings (Case 2) is larger than of that with 24-hour constant temperature settings (Case 1(a)). However, the total daily power consumption and daily energy cost of Case 1(a) is lower than Case 2. In both Case 1 and Case 2, the pump in the water system is operated at its nominal speed over the course of the 24-hour operation. The significant contribution of the pump's scheduling and operation in power consumption of the overall system is highlighted in Case 3 and Case 4, where the speed of the pump is varied and optimized based on the hour-ahead water demand and tank's water level forecasting. The findings verified that the economic dispatch including pump's speed varied within 0.5-1 p.u. results in the lowest power consumption and cost of operation per day. The pump's optimal setting eliminated the peaks in the pump's power consumption, and optimized the water demand response leading to less fluctuated tank's effluent which will improve the lifespans of the pump and tank's valves. By running the optimization model for EoD constraints of battery energy and tank's level from 20% to 100% of their nominal values for constant pump speed, it was found that $E_{batt}^{t_{end}} = 0.7E_{batt}^{max}$ and $Q_T^{t_{end}} = 0.9Q_T^{max}$ are optimal EoD values. Finally, lower battery efficiencies result in less utilization of the battery in the economic dispatch and increase the daily cost of the operation.

VII. Conclusion

In this paper, a mixed integer linear programming formulation was used to optimize the water consumption and thermal energy balance of a microgrid with diesel distributed generation, renewable energy sources, and storage units. Bivariate and univariate piecewise linearization were used to approximate the nonlinear optimization model to a linear programming formulation. It was concluded that daily cost of operation was significantly reduced if the indoor temperature settings of the buildings were set to 20-25°C the entire day. The daily cost increased when flexible indoor temperature settings of 15-30°C were used for the buildings during unoccupied hours. Such extra operating cost is much greater than the energy savings achieved as the result of the low/high temperature settings during the unoccupied times. However, the lowest energy cost was achieved if variable speed pump with normalized speed of 0.5-1p.u. and daily indoor temperature settings of 20-25°C were utilized for all the buildings. The daily cost increased when the battery efficiency reduced. In addition, enforcing the end-of-day battery energy and tank level constraints increase the daily cost of the system. Some of the limitations of the proposed model include: (i) the studied water distribution system is assumed to have no leakage, and in the case of a considerable leakage in the network, unforeseen tank

withdrawal can occur and (ii) the microgrid model does not account for electric vehicles. Future research will focus on optimal scheduling of energy-water networks considering the resilience against cyberattacks.

ACKNOWLEDGEMENT

The authors would like to acknowledge Penn State's Center for Security Research and Education (CSRE) for supporting this research through 2020 Homeland Security Award.

REFERENCES

[1] R. Connor, *The United Nations World Water Development Report 2015: Water for a Sustainable World*, vol. 1. Paris, France: UNESCO Publ., 2015,
[2] X. Zhang and V. V. Vesselinov, "Energy-water nexus: Balancing the tradeoffs between two-level decision makers," *Appl. Energy*, vol. 183, pp. 77–87, Dec. 2016.
[3] X. Zhang and V. V. Vesselinov, "Integrated modeling approach for optimal management of water, energy and food security nexus," *Adv. Water Resour.*, vol. 101, pp. 1–10, Mar. 2017.
[4] K. Oikonomou, M. Parvania, and R. Khatami, "Optimal demand response scheduling for water distribution systems," *IEEE Trans. Ind. Informat.*, vol. 14, no. 11, pp. 5112–5122, Nov. 2018.
[5] M. Li, Q. Fu, V. P. Singh, D. Liu, and T. Li, "Stochastic multi-objective modeling for optimization of water-food-energy nexus of irrigated agriculture," *Adv. Water Resour.*, vol. 127, pp. 209–224, May 2019.
[6] Y. Si, X. Li, D. Yin, T. Li, X. Cai, J. Wei, and G. Wang, "Revealing the water-energy-food nexus in the upper yellow river basin through multi-objective optimization for reservoir system," *Sci. Total Environ.*, vol. 682, pp. 1–18, Sep. 2019.
[7] K. Oikonomou and M. Parvania, "Optimal coordination of water distribution energy flexibility with power systems operation," *IEEE Trans. Smart Grid*, vol. 10, no. 1, pp. 1101–1110, Jan. 2019.
[8] J. A. Daw *et al.*, "Energy-water microgrid opportunity analysis at the university of arizona's biosphere 2 facility," Nat. Renew. Energy Lab. (NREL), Golden, CO, USA, Rep. NREL/TP-7A40-71294, 2018.
[9] E. Whitney *et al.*, "MicroFEWs: A food–energy–water systems approach to renewable energy decisions in islanded microgrid communities in rural Alaska," *Environ. Eng. Sci.*, vol. 36, no. 7, pp. 843–849, 2019.
[10] J. Najafi, A. Peiravi, A. Anvari-Moghaddam, and J. M. Guerrero, "An efficient interactive framework for improving resilience of power-water distribution systems with multiple privately-owned microgrids," *Int. J. Electr. Power Energy Syst.*, vol. 116, Mar. 2020, Art. no. 105550.
[11] F. Dubuisson, M. Rezkallah, A. Chandra, M. Saad, M. Tremblay, and H. Ibrahim, "Control of hybrid wind–diesel standalone microgrid for water treatment system application," *IEEE Trans. Ind Appl.*, vol. 55, no. 6, pp. 6499–6507, Nov./Dec. 2019.
[12] J. A. Aguilar-Jiménez, N. Velázquez, R. Beltrán, L. Hernández-Callejo, R. López-Zavala, and E. González-San Pedro, "Potential for thermal water desalination using microgrid and solar thermal field energy surpluses in an isolated community," in *Proc. Ibero-Amer. Congr. Inf. Manag. Big Data*, 2019, pp. 162–175.
[13] F. Moazeni, J. Khazaei, and J. P. P. Mendes, "Maximizing energy efficiency of islanded micro water-energy nexus using co-optimization of water demand and energy consumption," *Appl. Energy*, vol. 266, pp. 1–11, May 2020.
[14] M. Roustaei *et al.*, "A scenario-based approach for the design of smart energy and water hub," *Energy*, vol. 195, May 2020, Art. no. 116931.
[15] P. Venkataraman, *Applied Optimization with MATLAB Programming*. New York, NY, USA: Wiley, Mar. 2009.
[16] G. W. Chang, Y. D. Tsai, C. Y. Lai, and J. S. Chung, "A practical mixed integer linear programming based approach for unit commitment," in *Proc. IEEE Power Eng. Soc. Gen. Meeting*, vol. 1, 2004, pp. 221–225.
[17] P. Gautam, R. Karki, and P. Piya, "Probabilistic modeling of energy storage to quantify market constrained reliability value to active distribution systems," *IEEE Trans. Sustain. Energy*, vol. 11, no. 2, pp. 1043–1053, Apr. 2020.
[18] P. Mirhoseini and N. Ghaffarzadeh, "Economic battery sizing and power dispatch in a grid-connected charging station using convex method," *J. Energy Storage*, vol. 31, Oct. 2020, Art. no. 101651.
[19] "Energy performance of buildings—Calculation of energy use for space heating and cooling," ISO Standard 13790: 2008, 2008.
[20] X. Jin, Y. Mu, H. Jia, J. Wu, T. Jiang, and X. Yu, "Dynamic economic dispatch of a hybrid energy microgrid considering building based virtual energy storage system," *Appl. Energy*, vol. 194, pp. 386–398, May 2017.
[21] O. A. Zainal and R. Yumrutaş, "Validation of periodic solution for computing CLTD (cooling load temperature difference) values for building walls and flat roofs," *Energy*, vol. 82, pp. 758–768, Mar. 2015.
[22] R. J. Houghtalen, A. Osman, and N. H. Hwang, *Fundamentals of Hydraulic Engineering Systems*. New York, NY, USA: Prentice Hall, 2016.
[23] P. Bonami *et al.*, "An algorithmic framework for convex mixed integer nonlinear programs," *Discr. Optim.*, vol. 5, no. 2, pp. 186–204, 2008.
[24] T. Achterberg, "SCIP: Solving constraint integer programs," *Math. Program. Comput.*, vol. 1, no. 1, pp. 1–41, 2009.
[25] T. M. Walski, D. V. Chase, D. A. Savic, W. Grayman, S. Beckwith, and E. Koelle, *Advanced Water Distribution Modeling and Management*. Waterbury, CT, USA: Haestad Press, 2003.

Faegheh Moazeni received the Ph.D. degree in civil and environmental engineering from the University of Nevada Las Vegas (UNLV) in 2013. From 2013 to 2016, she was with Menlo Energy, Florida. She is currently a Faculty with the School of Science, Engineering and Technology, Penn State Harrisburg. Her research interests include smart water systems, water-energy nexus, and water system security against cyberattacks. She is an Associate Member of ASCE.

Javad Khazaei (Senior Member, IEEE) received the Ph.D. degree in electrical engineering from the University of South Florida in 2016. He is currently an Assistant Professor with the School of Science, Engineering and Technology, Penn State Harrisburg and is also affiliated with the Architectural Engineering Department, Penn State University. His research interests include cyber-physical power system modeling, control, and optimization, and smart grid security.

Arash Asrari (Senior Member, IEEE) received the Ph.D. degree in electrical engineering from the University of Central Florida, Orlando, FL, USA, in 2015. From 2015 to 2017, he was a Senior Consulting Engineer with Phasor Engineering, LLC, Florida. He is currently an Assistant Professor with the School of Electrical, Computer, and Biomedical Engineering, Southern Illinois University Carbondale, IL, USA. His current research interests include power systems optimization and smart grid security. He is currently an Associate Editor of IEEE ACCESS.